Supplementary Information

Tailoring Hierarchical MnO_2 Nanostructures on Self-Supporting Cathodes for High-Mass-Loading Zinc-Ion Batteries

Weijie Zheng [a], Zhibiao Cui [a], Cong Liu [c], Libei Yuan [d], Shengsong Li [a], Lilin Lin [a], Tao Meng [a]*, Liangui Yang [a], Yexiang Tong [c], Dong Shu [a,b]*

[a] School of Chemistry, South China Normal University, Guangzhou, 510006, People's Republic of China.

[b] National and Local Joint Engineering Research Center of MPTES in High Energy and Safety LIBs, South China Normal University, Guangzhou, 510006, People's Republic of China.

[c] MOE of the Key Laboratory of Bioinorganic and Synthetic Chemistry, The Key Lab of Low-Carbon Chemistry & Energy Conservation of Guangdong Province, School of Chemistry, Sun Yat-sen University, Guangzhou 510275, People's Republic of China.

[d] Institute for Superconducting and Electronic Materials, Australian Institute for Innovative Materials, University of Wollongong, Wollongong, NSW, 2522 Australia.

* Corresponding author: mengt@scnu.edu.cn; dshu@scnu.edu.cn

1. Experimental Section

1.1 Materials

All chemicals were analytically graded and used as received without further purification. Potassium permanganate (AR, $KMnO_4$) were purchased from Tianjin Damao chemical Reagent Co., Ltd.. Cetyltrimethylammonium bromide (AR, CTAB) were purchased from Shanghai Macklin Biochemical Co., Ltd.. Carbon carbon (CC) was received from Nanjing Xianfeng Nano Material Technology Co., Ltd..

1.2 Synthesis of MNSMO@CC and MO@CC cathode

The carbon cloth was cut into 3 cm x 3 cm pieces and subjected to an overnight acidic treatment using a mixture of H_2SO_4 and HNO_3 in a 3:1 ratio to obtain activated carbon cloth. To prepare the precursor solution, 0.1 mmol of CTAB was added to 40 mL of deionized (DI) water. The solution was stirred for 10 minutes using a magnetic stirrer. Subsequently, the activated carbon cloth was immersed in the solution and allowed to pre-adsorb CTAB molecules for 30 minutes. Then, 1 mmol of $KMnO_4$ was added to the solution and sonicated for 15 minutes. The solution was transferred to a 100 mL Teflon-lined stainless-steel autoclave, keep the temperature at 140 ℃ for 12 h, and cool at room temperature. After taking out the carbon cloth, the obtained MNSMO@CC was washed with DI water and ethanol three times, dried in an oven at 65 ℃ for 8 h. The mass loading of active substances on carbon cloth is ~ 2.0 mg cm^{-2} for normal tests and between 4.0-7.0 mg cm^{-2} for high mass loading tests. The reference samples (MO@CC) were prepared under the same conditions without the addition of CTAB.

1.3 Synthesis of Zn@CC anode

Flexible Zn@CC electrodes were obtained by electrodepositing Zn on carbon cloth, where the carbon cloth was used as the working electrode and Zn foil was employed as the reference and counter electrode. Electroplating was performed using CHI 660E at -0.8 V in a 1 M $ZnSO_4$ solution for 2700 s.[1]

1.4 Fabrication of Zn/MNSMO@CC battery and Zn@CC||MNSMO@CC pouch cell

The Zn/MNSMO@CC battery was assembled, and the prepared MNSMO@CC sample was cut into disks with a diameter of 10 mm as direct cathodes, and the same size Zn sheet (0.5mm) was cut as the anode. $ZnSO_4$ (2.0 M) solution with $MnSO_4$ (0.1 M) was used as electrolyte and the Glass fiber membrane (GF/D) was used as the separator. For the pouch cell, the MNSMO@CC was directly used as cathode without further cut. The Zn@CC and GF/D were used as anode and separator, and the Al-plastic films were used for packaging.

1.5 Materials Characterizations

Scanning electron microscopy (SEM, ZEISS Ultra-55) and transmission electron microscopy (TEM, FEI Talos F200X) were used to examine the morphology and structure of the synthesized samples. The phase purity and crystallinity of the prepared materials were examined by X-ray powder diffraction (XRD) on a Rigaku Ultima IV X-ray diffractometer in the 2θ range of 5 ~ 80° at a scan rate of 10° min^{-1}. The Raman spectra were carried out on a Raman spectrometer (inVia, λ = 514 nm). The surface area, pore volume, and pore diameter of the samples were analyzed via the Brunauer-Emmett-Teller (BET) method and Barrett-Joyner-Halenda (BJH) method, respectively. The surface chemical composition and valence of the samples were characterized using X-ray photoelectron spectroscopy (XPS, Axis Supra). Nitrogen adsorption and desorption isotherms were recorded at 77 K using a Micromeritics ASAP 2020 Plus analyzer. X-ray absorption near edge structure spectra were obtained by Rapid XAFS.

1.6 COMSOL Multiphysics simulation

The simulations were carried out using COMSOL Multiphysics with the Electric Current, Solid Mechanics and Solid Heat Transfer module through 3D models show in Figure S15. The average current density through the materials were set to 1 mA cm^{-2}, representing the electrochemical process of the electrode. The majority of the simulated structure consists of the CC fiber with a radius of 5 μm, and the covering

MnO_2 with a thickness of 0.4 μm.

1.7 DFT Calculations

All spin-polarized density functional theory (DFT) calculations were performed using the Vienna Ab Initio simulation package (VASP).[2] The GGA-PBE functional is selected for the exchange and correlation potential. All atoms relax completely until the remaining force on each atom was smaller than 0.03 meV $Å^{-1}$, and the energy convergence criterion is set to 10 ~ 5 eV. The adsorption energy (Eads) could be defined as the following formula:[3]

$$E_{adsorption} = E_{adsorbate/substrate} - E_{adsorbate} - E_{substrate} \quad (S1)$$

1.8 Molecular dynamics simulation

The diffusion of Zn in the MnO_2@CC systems was studied using the molecular dynamics (MD) method based on the Forcite module in Materials Studio. The canonical (NVT) ensembles with constant particles (N), a constant temperature of 298 K was chosen in our simulation. In the pristine MnO_2@CC system, 10 $ZnSO_4$ molecules, 280 H_2O molecules, and 50 MnO_2 were chosen in our simulation model. The total simulation time was 50 ps, and the time step was one fs. The diffusion coefficient (D) of the oxygen molecule was calculated according to the following formula[4]:

$$\langle r^2 \rangle = 6 D t + C \quad (S2)$$

where $\langle r^2 \rangle$ is the mean square distance (MSD) and t is time. D and C are constants, while D means the diffusion coefficient.

1.9 Electrochemical measurements

CV, GCD, and EIS measurements were recorded with CHI660E, at room temperature. Rate performance and cycle performance of Zn/MNSMO@CC batteries were recorded by the Neware battery test system (CT-4008-5V 10 mA).

To analysis the electrode kinetics for Zn storage, the cyclic voltammetry curves at different sweep rates were measured. Generally, the measured peak current (i) and sweep rate (v) in a CV scan obey a power-law relationship:[5]

$$i = av^b \quad (S3)$$

$$log(i) = log(a) + blog(v) \quad \text{(S4)}$$

where, *a* and *b* are adjustable, and the *b* value can be attained by fitting slope of the log(i) versus log(v) profile. A *b* value of 1.0 indicates a capacitive dominated charge storage behavior while a *b* value of 0.5 refers to ionic diffusion-controlled behavior. Furthermore, for a quantitative analysis of diffusion-controlled and capacitive contributions in current response, assumption of an integration of semi-infinite diffusion and capacitive like process were carried out by the following equation:[6]

$$i = k_1v + k_2v^{1/2} \quad \text{(S5)}$$

The diffusion-controlled and capacitive contributions can be estimated by determining k_1 and k_2.

The capacitive contribution was calculated by the following equation:

$$I_p = C_1v + C_2v^{1/2} \quad \text{(S6)}$$

where I_p is the peak current at different scan rates, v is the scan rate (mV s^{-1}), C_1 and C_2 are the constant factors corresponding to the capacity contribution of the surface pseudocapacitive effect and the battery-type effect, respectively.

The relationship between the structural variation and corresponding cathode kinetic properties of the diffusion coefficient of zinc ions (D_{Zn}^{2+}) were demonstrated by galvanostatic intermittent titration technique (GITT) measurements and were used to calculate based on the following equation:[7]

$$D_{Zn}^{2+} = \frac{4}{\pi\tau}\left(\frac{mv}{MA}\right)^2\left(\frac{\Delta Es}{\Delta Et}\right)^2 \quad \text{(S7)}$$

where *m* (g) and *M* (g mol^{-1}) are assigned to the loading mass and molecular weight of active material; v (cm^3 mol^{-1}) represents the molar volume of materials deduced from crystallographic data; τ (s) is constant current pulse time; *A* (cm^2) is the surface area of electrode; *ΔEs* (V) and *ΔEt* (V) denote the change of steady-state voltage and the total change of the voltage during a constant pulse for a single-step GITT curve, respectively. A current density of 100 mA g^{-1} is applied to the AZIBs with τ = 10 min and then stood for 60 min without current impulse.

2. Supplementary Figures

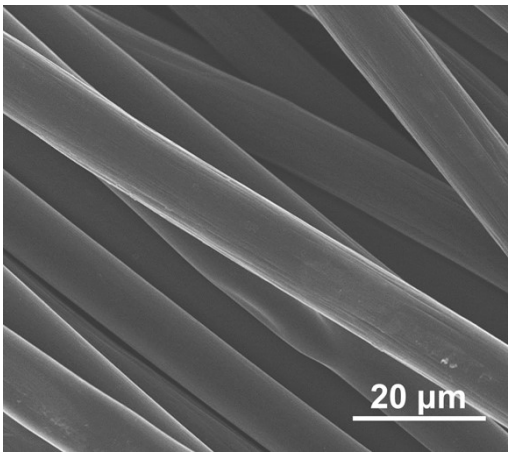

Figure S1. SEM image of the activated carbon cloth.

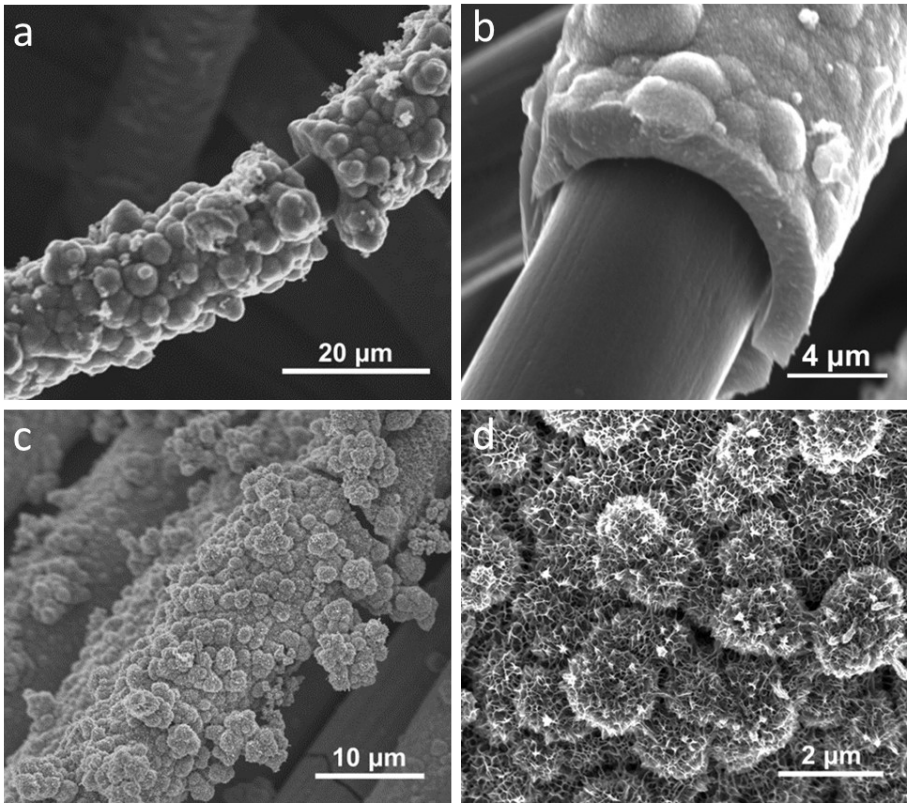

Figure S2. SEM images of (a-b) MO@CC and (c-d) MNSMO@CC.

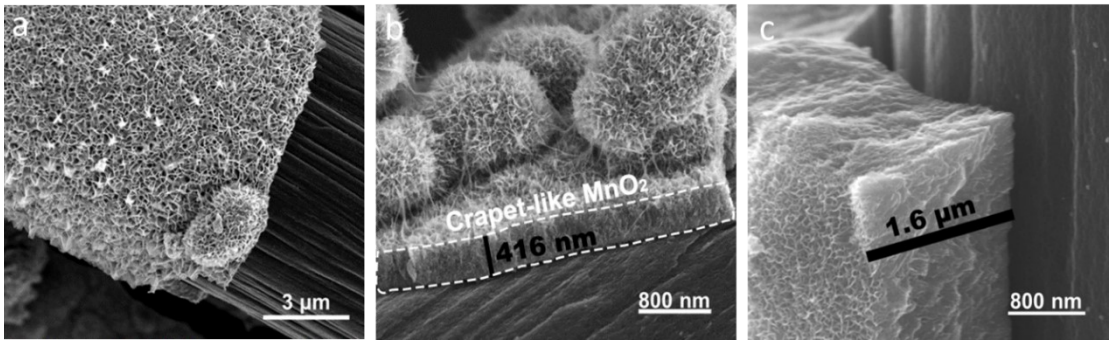

Figure S3. SEM images of (a-b) MNSMO@CC and (c) MO@CC.

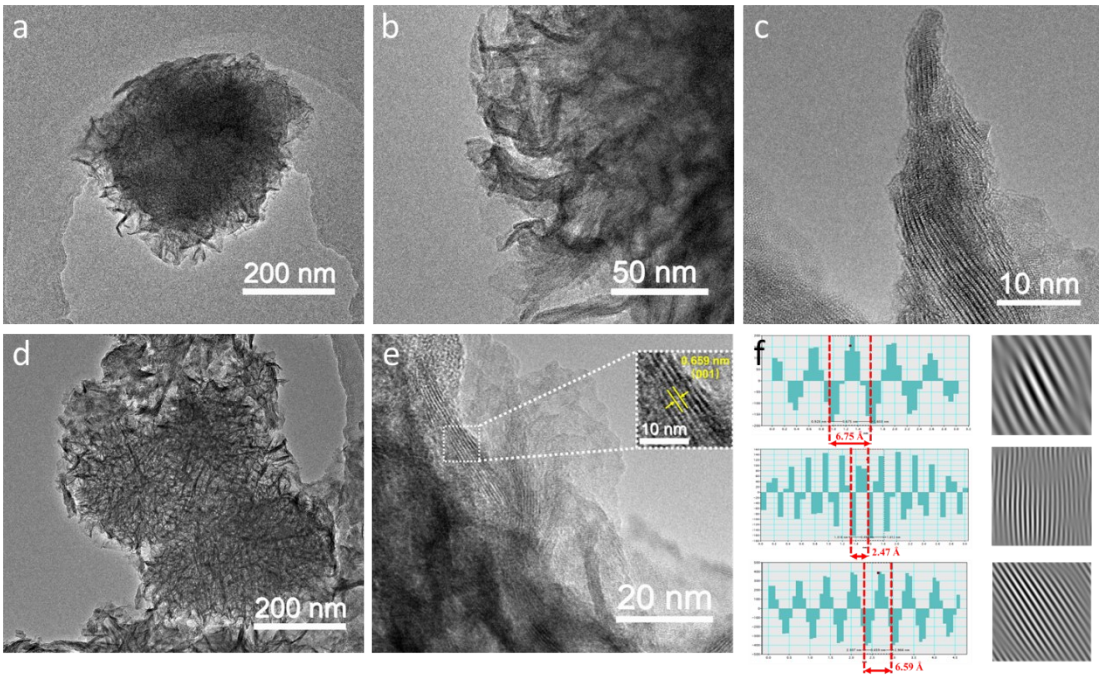

Figure S4. TEM images of (a-c) MNSMO@CC, and (d-e) MO@CC. (f) Inverse fast Fourier transform patterns of the white-rectangular area in Figure 1d, and Figure S4e.

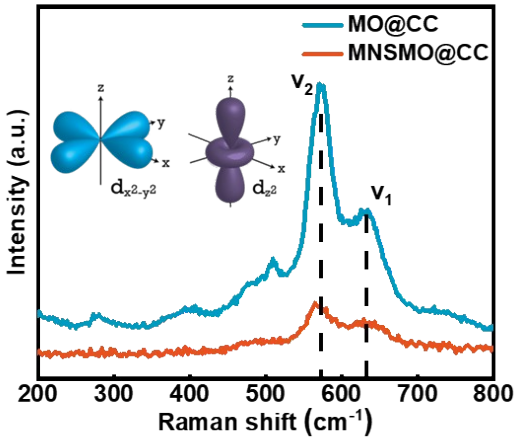

Figure S5. Raman spectra of MNSMO@CC and MO@CC

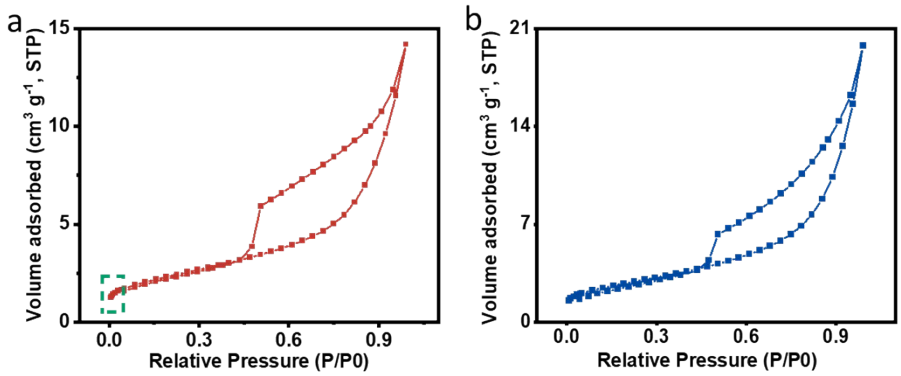

Figure S6. Nitrogen adsorption-desorption isotherms of (a) MNSMO@CC and (b) MO@CC.

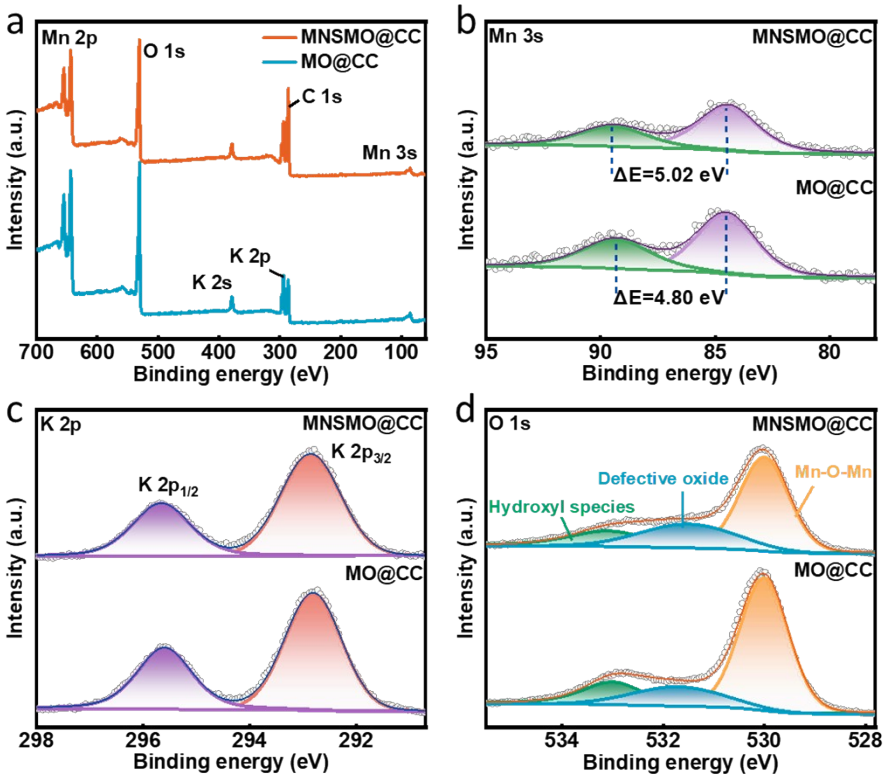

Figure S7. (a) X-ray photoelectron spectroscopy (XPS) survey spectrum. High-resolution XPS spectra of MNSMO@CC and MO@CC: (b) Mn 3s, (c) K 2p, and (d) O 1s.

The average oxidation state (AOS) is calculated according to the following empirical formula:

$$AOS = 8.956 - 1.126 \times \Delta E \quad \text{(S8)}$$

The ΔE is the energy splitting in these two samples. The doublet of K 2p spectra located at 292.85 eV (K $2p_{3/2}$) and 295.68 eV (K $2p_{1/2}$) (**Figure S7c**). The O 1s XPS spectra displays peaks located at 530.00, 531.50 and 533.10 eV, which are corresponded to the Mn-O-Mn bonding, oxygen defects and surface absorbed oxygen species, respectively (**Figure S7d**).

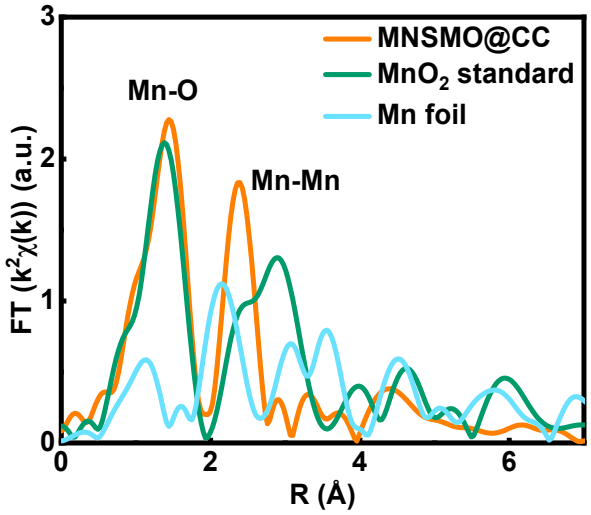

Figure S8. FT-EXAFS spectra for the Mn K-edge of MNSMO@CC, standard MnO_2, and Mn foil.

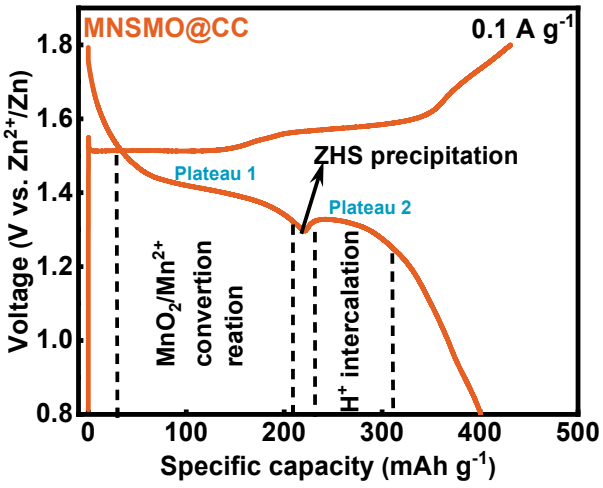

Figure S9. GCD curve of MNSMO@CC.

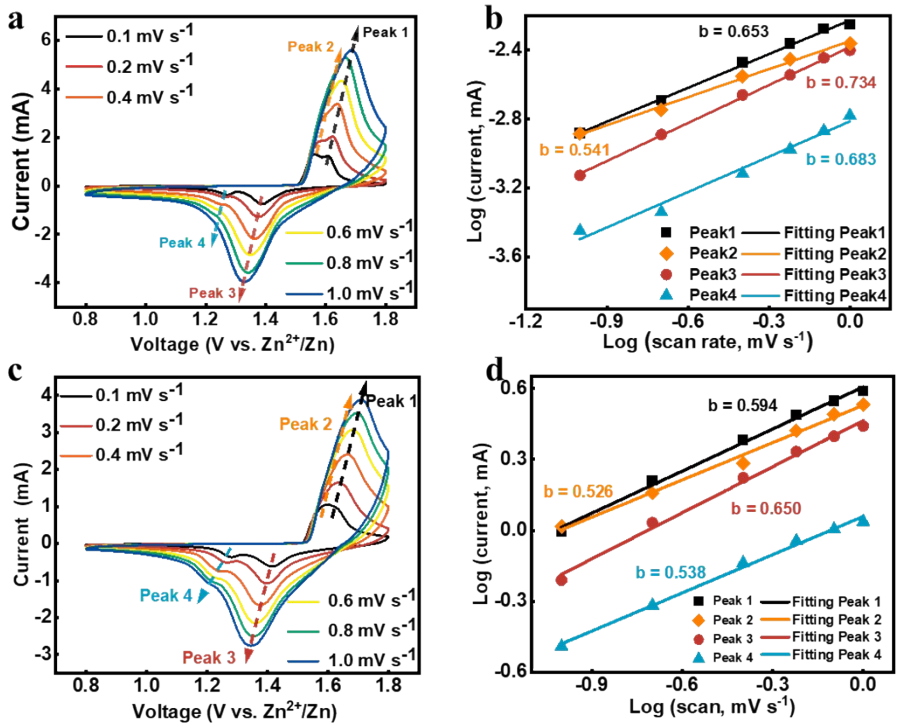

Figure S10. (a), (c) CV curves with different scan rate and (b), (d) log *i* versus log *v* plots at four peaks of MNSMO@CC and MO@CC electrodes.

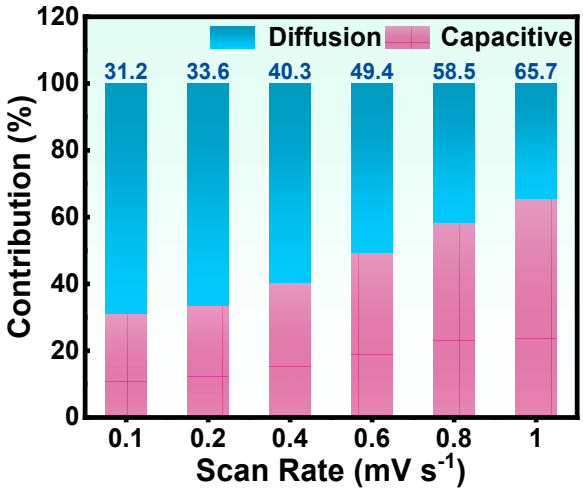

Figure S11. Diffusion coefficient values calculated of MO@CC.

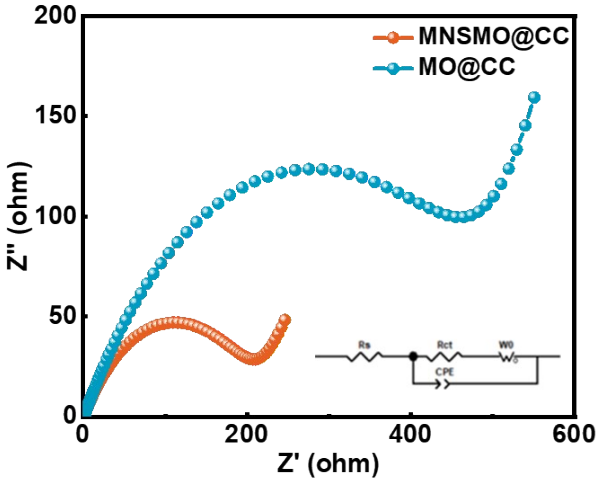

Figure S12. Nyquist plot of MNSMO@CC and MO@CC.

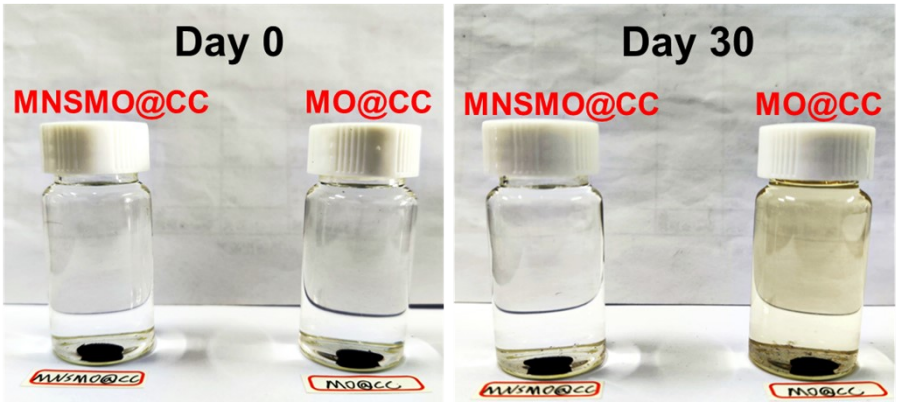

Figure S13. Immersion test of MNSMO@CC and MO@CC electrodes in electrolyte.

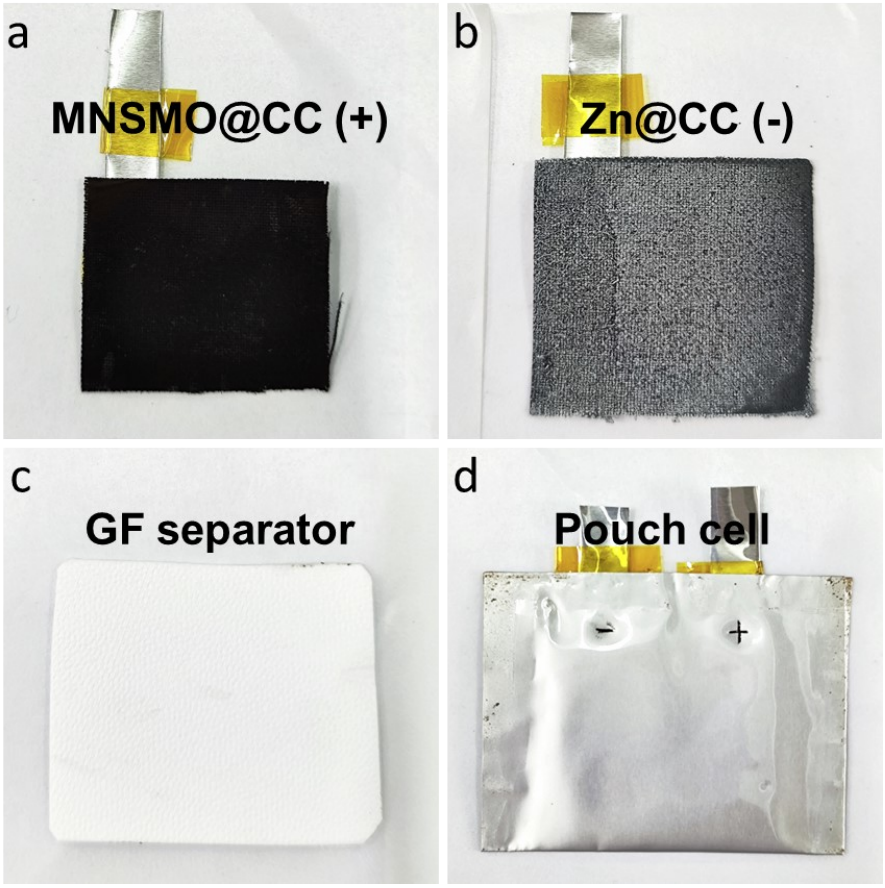

Figure S14. Schematic diagram of various components of soft pack battery.

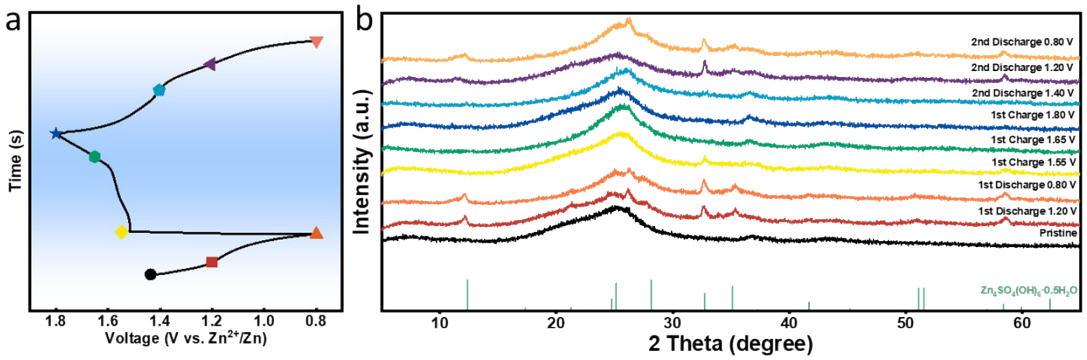

Figure S15. (a) GCD curves of the first cycle and the second discharge and (b) Corresponding ex situ XRD of the MNSMO@CC electrode.

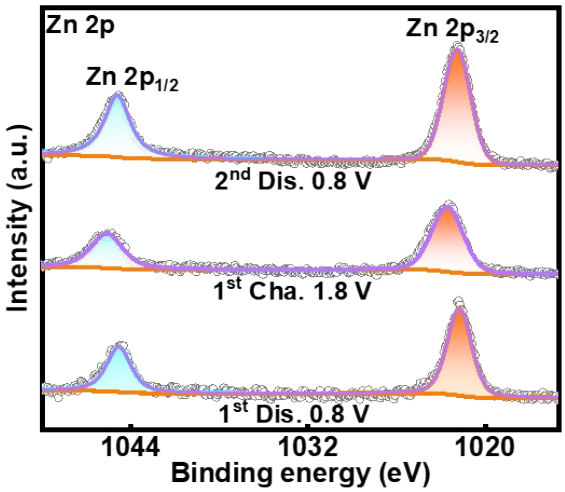

Figure S16. XPS spectra of Zn 2p.

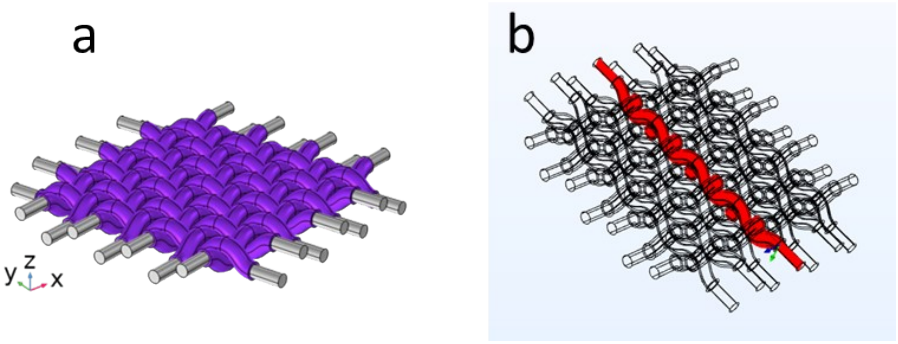

Figure S17. (a) COMSOL model of the carpet-like MnO_2 with carbon cloth. (b) the cross section of the model.

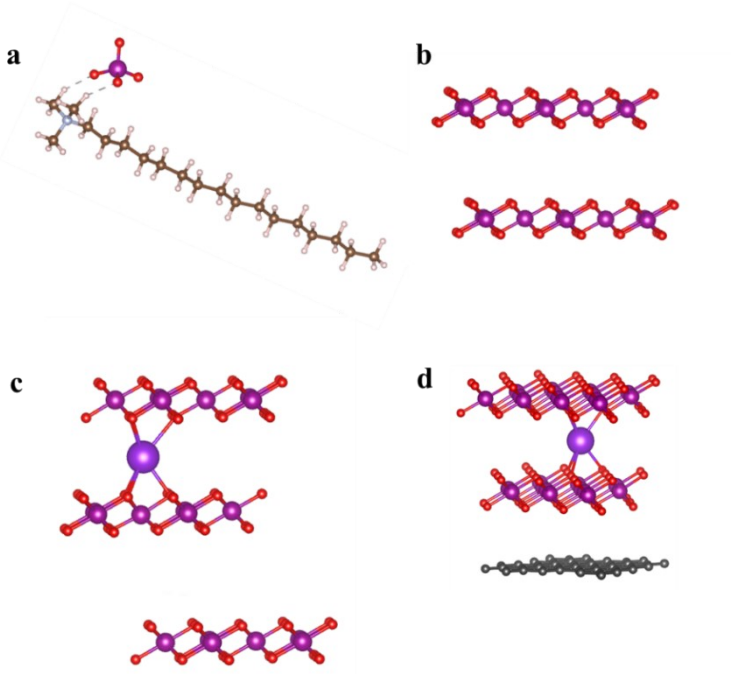

Figure S18. The DFT calculation models of (a) CTA^{+}-MnO_4^{-} molecular, (b) δ-MnO_2, (c) K-MnO_2, and (d) K-MnO_2@CC.

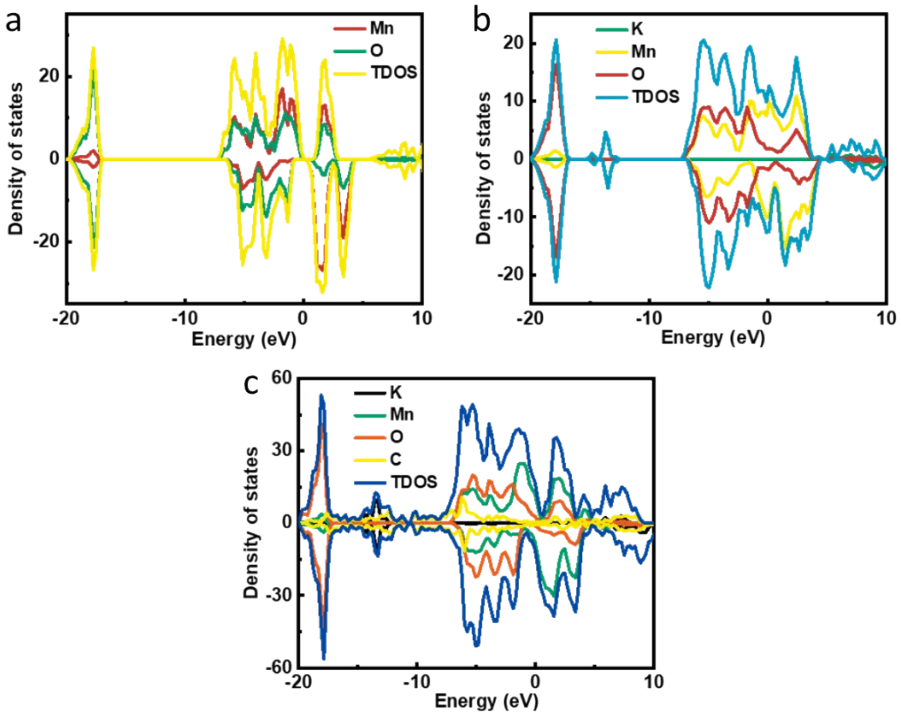

Figure S19. TDOS of (a) δ-MnO_2, (b) K-MnO_2, and (c) K-MnO_2@CC.

Table S1. The mass loading and electrochemical performance of different cathode.

Cathode	Mass loading (mg cm^{-2})	Current density (A g^{-1})	Current collector diameter (mm)	Areal capacity (mAh cm^{-2})	Ref.
VMP	0.5-0.6	0.5	10	0.22	[8]
γ-MnO_2@CP	2	0.1	14	0.52	[9]
PVP-MnO_2	0.7-1.5	0.125	11	0.5	[10]
MnO_2@AEPA	1-1.5	0.2	14	0.26	[11]
V_2O_5•1.75H_2O	1.2	0.1	14	0.47	[12]
ZnVO	1	0.1	12	0.37	[13]
H-VO_2	2	0.1	14	0.53	[14]
CMK-3@I_2	1.2-1.5	0.2	14	0.11	[15]
PC@Fe_2N-4/I_2	1-1.2	0.422	10	0.26	[16]
MNSMO@CC	**4-7**	**0.1**	**10**	**0.64**	**This work**

References

[1] T. Chen, F. Wang, S. Cao, Y. Bai, S. Zheng, W. Li, S. Zhang, S. X. Hu, H. Pang, *Adv. Mater.s* 2022, **34**, 2201779.

[2] J. Ling, A. Gao, Y. Huang, F. Yi, Q. Li, G. Wang, Y. Liu, D. Shu, *Chem. Eng. J.* 2023, **452**, 139661.

[3] Z. Cui, F. Yi, T. Meng, A. Gao, J. Hao, Y. Wang, S. Li, J. Huang, D. Shu, *Sustain. Mater. Technol.* 2023, **37**, e00678.

[4] D. Ma, Z. Zhao, Y. Wang, X. Yang, M. Yang, Y. Chen, J. Zhu, H. Mi, P. Zhang, *Adv. Mater.* 2024, **36**, 2310336.

[5] J. Zhang, W. Li, J. Wang, X. Pu, G. Zhang, S. Wang, N. Wang, X. Li, *Angew. Chem.*

Int. Ed. 2023, **62**, e202215654.

[6] L. Dai, Y. Wang, L. Sun, Y. Ding, Y. Yao, L. Yao, N. E. Drewett, W. Zhang, J. Tang, W. Zheng, *Adv. Sci.* 2021, **8**, 2004995.

[7] S. Cui, D. Zhang, Y. Gan, *Adv. Energy Mater.* 2024, **14**, 2302655.

[8] J. Chen, J. Liang, Y. Zhou, Z. Sha, S. Lim, F. Huang, Z. Han, S. A. Brown, L. Cao, D.-W. Wang, *J. Mater. Chem. A* 2021, **9**, 575.

[9] W. Lv, Z. Shen, X. Li, J. Meng, W. Yang, F. Ding, X. Ju, F. Ye, Y. Li, X. Lyu, *Nano-Micro Lett.* 2024, **16**, 109.

[10] A. Zhang, R. Zhao, Y. Wang, J. Yue, J. Yang, X. Wang, C. Wu, Y. Bai, *Angew. Chem. Int. Ed.* 2023, **62**, e202313163.

[11] X. Xiao, L. Zhang, W. Xin, M. Yang, Y. Geng, M. Niu, H. Zhang, Z. Zhu, *Small* **2024**, 2309271.

[12] K. Zhu, T. Wu, K. Huang, *Energy Storage Mater.* **2021**, 38, 473.

[13] Z. Pang, B. Ding, J. Wang, Y. Wang, L. Xu, L. Zhou, X. Jiang, X. Yan, J. P. Hill, L. Yu, Y. Yamauchi, *Chem. Eng. J.* 2022, **446**, 136861.

[14] K. Zhu, T. Wu, S. Sun, W. van den Bergh, M. Stefik, K. Huang, *Energy Storage Mater.* 2020, **29**, 60.

[15] Q. Guo, H. Wang, X. Sun, Y. N. Yang, N. Chen, L. Qu, *ACS Mater. Lett.* 2022, **4**, 1872.

[16] Q. Chen, S. Chen, J. Ma, S. Ding, J. Zhang, *Nano Energy* 2023, **117**, 108897.